Emission characteristics of primary brown carbon absorption from biomass and coal burning: Development of an optical emission inventory for China

Jie Tian[1,2], Qiyuan Wang[2], Haiyan Ni[2], Meng Wang[2], Yaqing Zhou[2], Yongming Han[2,3], Zhenxing Shen[1], Siwatt Pongpiachan[4], Ningning Zhang[2], Zhuzi Zhao[2], Qian Zhang[1], Yue Zhang[1], Xin Long[2], Junji Cao[2,5]

[1] Department of Environmental Science and Engineering, School of Energy and Power Engineering, Xi'an Jiaotong University, Xi'an 710049, China.

[2] Key Laboratory of Aerosol Chemistry and Physics, State Key Laboratory of Loess and Quaternary Geology, Institute of Earth Environment, Chinese Academy of Sciences, Xi'an 710061, China.

[3] School of Human Settlements and Civil Engineering, Xi'an Jiaotong University, Xi'an 710049, China.

[4] School of Social & Environmental Development, National Institute of Development Administration (NIDA), Bangkok 10240, Thailand.

[5] Institute of Global Environmental Change, Xi'an Jiaotong University, Xi'an 710049, China.

Corresponding author: Junji Cao (cao@loess.llqg.ac.cn), Qiyuan Wang (wangqy@ieecas.cn) and Zhenxing Shen (zxshen@mail.xjtu.edu.cn)

Key Points:

- Brown carbon contributes 15–18% to the total particles light absorption at 370 nm from residential coal burning based on $AAE_{BC} = 1.0$.

- Residential coal burning has lower absorption emission factors of brown carbon at 370 nm than biomass burning.

- High-resolution maps of optical emission inventories for biomass and residential coal burning were developed for China.

Abstract

Brown carbon (BrC) affects the Earth's radiative balance due to its strong light absorption at short wavelengths. A custom-made combustion chamber was used to simulate biomass and coal burning and to investigate the emission characteristics of BrC absorption. Absorption Ångström exponents (AAEs) at the wavelength pair of 370 and 880 nm ranged from 1.19 to 3.25, suggesting the possible existence of BrC in biomass- and coal-burning emissions. Based on the assumption that $AAE_{BC} = 1.0$, BrC from biomass burning contributed to 41–85% of the total particles light absorption at 370 nm, which is much higher than that from coal burning (15–18%). The estimated absorption emission factors of BrC (AEF_{BrC}) at 370 nm for biomass and coal burning were 15–47 and 2–13 m^2 kg^{-1}, respectively. A 10 km $\times$ 10 km gridded BrC optical emission inventory for biomass and coal burning in China for 2015 was developed based on the measured AEF_{BrC} values and high-resolution activity data. The total annual BrC absorption cross section (ACS_{BrC}) emissions from biomass and residential coal burning were 4194 Gm^2 (relative uncertainty at the 95% confidence level of -33.2, 41.2%) and 615 Gm^2 (-39.3, 40.1%), respectively. These results should be useful for improving estimates of the radiative effects of BrC in China.

1. Introduction

Organic aerosol (OA) is a major component of the fine particulate matter that affects regional and global climate directly and indirectly, but the difficulties in constraining its light absorbing effects have caused large uncertainties in global radiative forcing assessments (IPCC, 2013). In the past, OA was considered a light scattering component only, and that effect would have tended to cool the atmosphere (Koch et al., 2007; Myhre et al., 2008). However, recent field measurements and laboratory studies have revealed that some OA chromophores can absorb solar radiation in the near-ultraviolet (UV) and short-visible regions of the spectrum (Kirillova et al., 2014; Kirchstetter and Thatcher, 2012; Saleh et al., 2013; Sun et al., 2007; Zhang et al., 2011). This light-absorbing fraction of OA is collectively termed brown carbon (BrC) (Andreae and Gelencsér, 2006). Recent modeling studies also have shown that the contribution of BrC to the total atmospheric absorption at ultraviolet/visible wavelengths may be considerable, and this perturbation could lead to heating of the atmosphere (Chuang et al., 2012; Feng et al., 2013; Jo et al., 2016; Lin et al., 2014; Saleh et al., 2015; Wang et al., 2014). However, the calculated direct radiative forcing (DRF) estimates for BrC have varied widely among studies. For example, Wang et al. (2014) estimate a much lower forcing for BrC (+0.04 to +0.11 W m^{-2}) than what was reported by Feng et al. (2013) (+0.1 to +0.25 W m^{-2}) and Lin et al. (2014) (+0.22 to +0.57 W m^{-2}). Results from such studies require a thorough understanding of the optical properties of BrC, which have not been thoroughly investigated and can vary dramatically among sources.

Biomass burning has been recognized as a dominant source of BrC worldwide (Chen and Bond, 2010; Clarke et al., 2007; Kirchstetter et al., 2004; Saleh et al., 2013; Washenfelder et al., 2015). With large agricultural sectors, China has expansive cultivated areas (166 million hectares) and enormous agricultural crop yields (781 Tg year^{-1}) (1 Tg = 10^{12} g), especially in the major agricultural zones shown in Supporting Information (SI) Figure S1a (NBS, 2016a). The North China Plain (zone 1, Shandong, Henan, Anhui, and Jiangsu Provinces) is the largest agricultural zone in China accounting for ~25% of the cultivated land and 25% of the crop yields. Another notable agricultural zone is composed of Heilongjiang, Jilin, and Liaoning Provinces in northeast China, where > 15% of the agricultural crops grown in China are produced annually. Zone 3, including Guangxi and Guangdong Provinces, accounts for more than 80% of sugarcane output (16% of the total crop products) in China. These agricultural areas produce tremendous amounts of crop

residues every year, which are commonly burned directly in the fields to prepare for the next plantings or used as energy sources for household cooking and heating (Zhou et al., 2017). Moreover, coal combustion is another source that can produce large quantities of BrC (Olson et al., 2015; Yan et al., 2017). In China, ~8.4% of the total coal burned (940 Tg) in 2015 is used for household heating and cooking purposes (NBS, 2016b). Poor combustion conditions and the lack of controls for residential coal burning lead to high BrC emissions from this source (Sun et al., 2017). As shown in SI Figure S1b, large amounts of coal are burned for residential purposes (20.5 Tg) in the Beijing-Tianjin-Hebei region (BTH) in 2015; this is one of the largest and most dynamic economic zones in China. The main coal-producing provinces (Shanxi and Guizhou Provinces) follow the BTH with consumption of 9.3 and 7.4 Tg year^{-1}, respectively. The provinces with lower residential consumption are concentrated in southern China; these include Fujian, Guangxi, Jiangsu, and Hainan Provinces.

Numerous studies have investigated the chemical composition and optical properties of BrC in the atmosphere using filter sampling/solvent extraction methods or photoacoustic instruments, but only a few studies have focused on the source emission characteristics of BrC (Chen and Bond, 2010; Kirchstetter et al., 2004; Li et al., 2016b; Mcmeeking et al., 2015; Pokhrel et al., 2016; Pokhrel et al., 2017; Saleh et al., 2013). Furthermore, the characterization studies have mainly focused on absorption Ångström exponent (AAE), the relative importance of BrC absorption versus BC, and quantifying of mass absorption cross section of BrC (MAC$_{BrC}$). To further understand the emission sources and develop effective strategies for air pollution control, BrC emission inventories for different sources are needed, but few studies have concentrated on the emission factors and rates at which BrC is produced during the burning of biomass and coal (Martinsson et al., 2015; Sun et al., 2017). This makes it challenging to evaluate accurately the radiative effects of combustion sources over regional and global scales, and more generally, to assess the impacts of BrC on climate and environment.

In the past two decades, multi-scale mass emission inventories for carbonaceous aerosols have been established for China using both bottom-up and top-down methods (Fu et al., 2012; Wang et al., 2012; Yan et al., 2006; Zhang et al., 2009). These types of inventories are useful for air quality modeling, especially simulations of the formation and transport of pollutants (Li et al., 2013). With regard to aerosol radiative effects, such inventories are also useful for calculating the carbonaceous DRF, but these effects are typically based on assumed relationships between carbonaceous masses and their optical properties (Yao et al., 2017; Zhang et al., 2014). Compared with mass emission inventories, there are at least two advantages for the development of optical emission inventories for use in models that simulate the BrC's radiative effects. One advantage is that it is not necessary to quantify the BrC mass. Due to the complex chemical composition of BrC (Laskin et al., 2014), complete quantitation of its mass is not possible with the current analytical methods. One of the major analytical challenges in quantifying BrC is developing a suitable separation procedure for distinguishing BrC chromophores from other aerosol constituents (Chen and Bond, 2010; Lack et al., 2013; Lin et al., 2015; Wonaschütz et al., 2009; Zhang et al., 2013). Several studies have used water-soluble organic carbon or humic acid sodium salt as proxies for BrC to obtain their emission factors (Srinivas and Sarin, 2014; Sun et al., 2017). However, these components may only be representative of certain fractions of BrC, and therefore, if one uses these empirically measured emission factors to establish mass emission inventories of BrC, the true BrC emissions may be underestimated. Another advantage is that an optical emission inventory can reduce the uncertainties caused by the mass absorption cross section of BrC (MAC$_{BrC}$) that are used in the models (Lu et al., 2015). The MAC$_{BrC}$ is a key parameter in models, and it is used to convert the masses of carbonaceous aerosols into their light-

absorbing properties, but this parameter has varied substantially among studies (e.g., 0.7–5.38 m^2 g^{-1} in the UV region) (Cheng et al., 2011; Kirchstetter et al., 2004; Shen et al., 2016; Srinivas and Sarin, 2014), and thus, it introduces uncertainties into the modeling calculation. In these respects, an optical emission inventory for China should be valuable for modeling purposes because it would reduce uncertainties in the radiative effects caused by BrC.

The main motivation of this study was to investigate the characteristics of BrC absorption and the optical emission factors from biomass and residential coal burning in China. Representative types of biomass and coals in China were burned using laboratory simulation methods. The optical properties measured with an Aethalometer were used to calculate the AAE and then to distinguish the BrC absorption from BC. Finally, based on the measured absorption emission factors of BrC and fuel consumption, we developed an optical emission inventory of BrC for China. The results should be useful for improving estimates of the radiative effects of BrC in China.

2. Materials and Methods

2.1. Combustion chamber experiments

The test burns for biomass and coal were done with the use of a custom-made combustion chamber, and a diagram of the experimental system is shown in SI Figure S2. Briefly, the test system consisted of a ~8 cubic meter cavity container. It was equipped with a thermocouple, a thermoanemoneter, and an air purification system. A dilution sampler (Model 18, Baldwin Environmental Inc., Reno, NV, USA) was installed downstream of the chamber to dilute the smoke before sampling. The combustion chamber was sealed against gas/particle loss (< 2% CO_2 losses after 30 minutes), flow was stable and uniform in the stack (< 5% variations of the average flow velocity), and clean and purified air was used for dilution (> 95% removal efficiency for background $PM_{2.5}$). The reproducibility and comparability of the emission factors of $PM_{2.5}$, OC, and EC have been demonstrated for replicate test measurements of wheat straw burning, and detailed description of the structure and an evaluation of the combustion chamber can be found in Tian et al. (2015).

Seven types of crop residues, including wheat straw, corn stalk, rice straw, soybean straw, cotton stalk, sesame stalk, and sugarcane top were collected from seven major Chinese crop producing provinces (SI Table S1). These were individually burned on the platform situated inside the chamber. Moreover, two representative types of coals, including high volatile bituminous coal (hv-coal) and low volatile bituminous coal (lv-coal), were collected from coal producing areas of Shaanxi and Ningxia, respectively (SI Table S1). Coal test burns were conducted in a typical stove that is widely used in northern China.

Smoke produced by biomass or coal burning was first diluted with the dilution sampler before it was monitored by several on-line instruments downstream (SI Figure S2). Recent laboratory studies have showed that "secondary BrC" can be produced in the multiphase reactions involving gas- and particle-phase compounds, and this can be an important source for BrC in the atmosphere (De Haan et al., 2011; Nguyen et al., 2012; Nozière et al., 2007; Powelson et al., 2014). The sampling procedure in our study took about 15 seconds for the source emissions to be sampled, and there were no conditions (e.g., relative high humidity, UV lights, etc.) that favored the formation of secondary BrC. Thus, we considered the measured BrC to be dominated by primary emissions. The dilution ratios were set at ~5–20 for most of burning experiments because those dilutions provided the appropriate pollutant concentration levels for on-line monitoring instruments. That procedure also simulates the rapid dilution and condensation that occurs naturally when source emission

mix with the atmosphere (Chang et al., 2004; Li et al., 2007; Li et al., 2011; Lipsky and Robinson, 2005; Lipsky and Robinson, 2006). For our studies, at least three parallel tests were conducted for each type of biomass or coal samples. A total of 45 tests were conducted as follows: 6 for each type of wheat straw, corn stalk, rice straw, soybean straw, cotton stalk, and sesame stalk and 3 for each type of sugarcane top, hv-coal, and lv-coal. When the aerosol deposit density on the filter tape in the Aethalometer reached the maximum attenuation, the filter tape automatically advanced. Advancing the filter tape took 5 minutes, and during that time, no measurements were made. Due to the tape advances of Aethalometer, ~20% of burning cases were found lacking of several 5-minutes data points during the sampling process. For discussion purposes, we only chose those burns that had intact measurements. Therefore, only 30 tests for biomass burning and 6 tests for coal combustion were left. Detailed information on each test burn is summarized in SI Table S1.

2.2. Modified combustion efficiency (MCE)

Different combustion conditions (e.g., flaming versus smoldering) could be differentiated by the MCE. MCE is typically close to 1 during the flaming phase, and ranges between 0.7 and 0.9 for the smoldering phase (Yokelson et al., 1997):

$$MCE = \frac{\Delta CO_2}{\Delta CO_2 + \Delta CO} \tag{1}$$

where ΔCO_2 and ΔCO were the excess molar mixing ratios of CO_2 and CO, respectively. CO_2 and CO concentrations of the diluted smokes were monitored by CO_2 sensors (PP Systems, Amesbury, MA, USA) and a CO analyzer (Thermo 48i, Thermo Scientific Inc., Franklin, MA, USA).

2.3. Calculation of AAE and quantification of BrC absorption

A newly developed Aethalometer (model AE33, Magee Scientific, Berkeley, CA, USA) was used to measure particles' light absorption at seven different wavelengths ($\lambda = 370$, 470, 525, 590, 660, 880, and 940 nm). A detailed description of this instrument and evaluation of it can be found in Drinovec et al. (2015). Briefly, the model AE33 measures the light attenuation transmitted through a quartz-fiber filter on which aerosol particles have been collected. Previous studies have demonstrated that the filter-based absorption photometers suffer from nonlinear loading effect as increasing amount of aerosol deposit on the filter (Weingartner et al., 2003). To improve the accuracy of absorption measurements, the model AE33 uses a real-time loading effect compensation algorithm based on a two parallel spot measurement of optical absorption. Both spots obtain their loadings from the same input air stream but with different deposition rates, and the results of these two sample spots are then combined to eliminate the nonlinearity effect. Additionally, the filter matrix scattering effect was modified automatically in AE33 by using a factor of 2.14 for quartz filter (Drinovec et al., 2015).

The wavelength (λ) dependence of particles' light absorption (b_{abs}) has been often described assuming a power law as follows (Andreae and Gelenscér, 2006; Hecobian et al., 2010):

$$b_{abs} \sim \lambda^{-AAE} \tag{2}$$

In practice, the AAE can vary depending on the selection of wavelength ranges (Moosmüller et al., 2011). In this study, AAE was calculated from two wavelengths of 370 and 880 nm, according to:

$$\text{AAE} = -\frac{\ln(\frac{b_{\text{abs}}(\lambda_1)}{b_{\text{abs}}(\lambda_2)})}{\ln(\frac{\lambda_1}{\lambda_2})} \qquad (3)$$

where b_{abs} is the total light absorption coefficient at a given wavelength; λ_1 of 370 nm was chosen due to strong contribution of BrC at this wavelength (Lack and Langridge, 2013); while λ_2 of 880 nm was chosen as the reference wavelength because BC can be considered as the only light-absorbing carbonaceous component at that wavelength (Kirchstetter et al., 2004; Kirchstetter and Thatcher, 2012). For comparison, AAE was also calculated by fitting the b_{abs} across all the six wavelengths (370, 470, 525, 590, 660, and 880 nm), and those results were similar to the those calculated for the 370 and 880 nm wavelength pair (SI Figure S3).

Generally, BC-absorption varies weakly with wavelength in the near-UV to infrared range showing an AAE around 1.0, though several studies have shown that the AAE of BC can vary from 0.55 to 1.6 (Bahadur et al., 2012; Bergstrom et al., 2002; Bond and Bergstrom, 2006; Lack and Cappa, 2010). In contrast, BrC absorbs radiation efficiently toward near-UV range (Schnaiter et al., 2006), and it has an AAE much greater than 1.0 in that region of the spectrum (Clarke et al., 2007; Hoffer et al., 2006; Kirchstetter et al., 2004).

In this study, the total b_{abs} at each wavelength (λ) can be separated into the absorption caused by BrC ($b_{\text{abs-BrC}}$) and BC ($b_{\text{abs-BC}}$). Thus, the $b_{\text{abs-BrC}}$ can be calculated using the following formula:

$$b_{\text{abs-BrC}}(\lambda) = b_{\text{abs}}(\lambda) - b_{\text{abs-BC}}(\lambda) \qquad (4)$$

where $b_{\text{abs}}(\lambda)$ was measured with the model AE33; b_{abs} at $\lambda = 880$ nm was assumed to be solely from the BC aerosol (Kirchstetter et al., 2004), and then extrapolated to calculate $b_{\text{abs-BC}}$ in other wavelengths ($\lambda = 370, 470, 525, 590,$ and 660 nm). The extrapolations were based on the assumption that $\text{AAE}_{\text{BC}} = 1.0$ (Bergstrom et al., 2002; Bond and Bergstrom, 2006) as follows:

$$b_{\text{abs-BC}}(\lambda) = b_{\text{abs-BC}}(880 \text{ nm}) \times \left(\frac{\lambda}{880}\right)^{-\text{AAE}_{\text{BC}}} \qquad (5)$$

The uncertainties for calculation of b_{abs} for BrC and BC are primarily caused by the uncertainty in AAE_{BC} and the measurement error of the model AE33. There was no pre-conditioning of the aerosol to remove coating in our tests, and therefore, the assumed AAE_{BC} was for BC internally mixed with non-absorbing material. The AAE method is used for attributing light absorption to BC plus lensing and BrC where internal mixing is largely ignored (Nakayama et al., 2014; Pokhrel et al., 2017). Here, absolute uncertainties of -20% and +40% were adopted to simulate AAE_{BC} over a range from 0.8 to 1.4 (Lack and Langridge, 2013). The relative uncertainty of absorption measurements of the model AE33 is $\pm 5\%$ (Titos et al., 2015). Through BrC and BC absorption attribution calculated formulas, the relative uncertainties of $b_{\text{abs-BC}}$ were estimated with the range of [-18%, +35%] at 370 nm, [-14%, +26%] at 470 nm, [-12%, +21%] at 525 nm, [-9%, +17%] at 590 nm, [-8%, +13%] at 660 nm, and [-5, +5%] at 880 nm, respectively. The relative uncertainty of $b_{\text{abs-BrC}}$ can be assessed by combining uncertainty of $b_{\text{abs-BC}}$ with the measurement error of the model AE33, and it varies with the fractional contribution of BrC to the total particles light absorption. A detailed description of the relative uncertainties in $b_{\text{abs-BrC}}$ and $b_{\text{abs-BC}}$ can be found in SI Text S1.

2.4. Absorption emission factor calculation

The emission factor, expressed as the weight of pollutant per kg of fuel consumed, is useful for assessing emission intensities of pollutants and for developing emission inventories

(Bond et al., 2004). Here, we define a term "absorption emission factor" (AEF) to determine the emission ability of $b_{abs-BrC}(\lambda)$ and $b_{abs-BC}(\lambda)$. The AEF represents the absorption cross section (m^2) emitted to the atmosphere per kg of fuel consumed, and it is calculated as:

$$\mathrm{AEF}_i\ (\lambda)\ [\mathrm{m^2\ kg^{-1}}] = \frac{\sum_{t=1}^{t=t_{sample}} b_{abs-i}(t)\ (\lambda)\ [\mathrm{m^{-1}}] \times \mathrm{DR} \times \mathrm{Vel}\ [\mathrm{m\ s^{-1}}] \times \mathrm{D}\ [\mathrm{m^2}]}{\mathrm{M}\ [\mathrm{kg}]} \qquad (6)$$

where subscript i represents BrC or BC; λ denotes the wavelength (370, 470, 525, 590, 660, or 880 nm); t_{sample} is the sampling duration in seconds; b_{abs-i} denotes the absorption coefficient of BrC or BC in $\mathrm{m^{-1}}$; DR is the dilution ratio (unitless); Vel is the average stack flow velocity in $\mathrm{m\ s^{-1}}$; D is the stack cross section in $\mathrm{m^2}$; M is the biomass or coal consumption in kg. All the data were standardized at the temperature of 293 K and pressure of 1013.25 hPa.

2.5. Development of an optical emission inventory

SI Figure S4 illustrates the methodology used to develop high-resolution emission inventories of BrC absorption cross section ($\mathrm{ACS_{BrC}}$) at 370 nm for biomass and residential coal burning in China. Note that the $\mathrm{ACS_{BrC}}$ emission from biomass burning in this study does not include wildfire emissions which also can be an important source for BrC (Forrister et al., 2015; Laing et al., 2016). Our approach made use of provincial-level emissions and proxy variables (fire counts, urban population, and rural population) as follows. First, the total quantities of biomass and residential coal burned in each province were estimated according to data obtained from the China Statistical Yearbook (2016) and the China Energy Statistical Yearbook (2016) (SI Text S2). Provincial-level emission inventories were then established by multiplying specific $\mathrm{AEF_{BrC}}$ values by the corresponding activity data (Chow et al., 2010). In addition, fire counts of croplands for 2403 counties in China in 2015 were obtained from the Moderate Resolution Imaging Spectroradiometer (MODIS) Thermal Anomalies/Fire product (MOD/MYD14A1), and rural/urban population statistics were taken from the fifth population census in China (SI Table S2). Based on the values of proxy variables (fire counts and population), the $\mathrm{ACS_{BrC}}$ emissions in each province were further allocated to county-level using the following formula (Qin and Xie, 2011):

$$\mathrm{E}_{i,j} = \frac{\mathrm{P}_{i,j}}{\sum_{i=1}\mathrm{P}_{i,j}} \times \mathrm{E}_j \qquad (7)$$

where $\mathrm{E}_{i,j}$ is the emission in county i of province j; $\mathrm{P}_{i,j}$ is proxy variable in county i of province j; and E_j is the emission in province j.

After allocating the provincial emissions to their counties, the national optical emission inventory at the county-level was disaggregated into grid cells at a resolution of 10 km × 10 km. The ratios of the area in each cell to the total county area were calculated to allocate the emission of the county to each grid cell. If a grid cell included more than one county, the emission for that grid cell is considered as the sum of emissions from different counties based on the calculated ratios.

3. Results and Discussion

3.1. Absorption Ångström exponent and BrC absorption

SI Figure S5 shows the AAEs obtained from the experimental burning of crop residues and bituminous coals along with the b_{abs} values for the wavelength pair of 370 and 880 nm. For crop residues, AAEs were in the range of 1.64 to 3.25, with the highest for corn stalk emissions (3.25 ± 0.36), followed by the wheat straw (2.99 ± 0.36), rice straw (2.70 ± 0.23), cotton stalk (2.69 ± 0.24), sesame stalk (2.40 ± 0.34), soybean straw (2.37 ± 0.15), and

sugarcane top (1.64 ± 0.15). For bituminous coal, AAEs were similar for hv-coal (1.19 ± 0.04) and lv-coal (1.26 ± 0.04) emissions. These AAEs, all > 1.0, suggest that particulate matter emitted from both crop residues and coal burning might contain BrC (Li et al., 2016b; Pandey et al., 2016; Shen et al., 2016; Sun et al., 2017). The AAEs obtained from crop residues were significantly higher compared with those from bituminous coals at 95% confidence level (student's t-test, $p < 0.001$). Utry et al. (2014) found that a positive correlation existed between AAEs and OC/EC (organic carbon/elemental carbon) ratios, and the large AAEs for crop residues found in this study may be explained by their higher OC/EC ratios compared with coals as measured in our previous studies (Ni et al., 2015; Tian et al., 2017).

To investigate the impacts of combustion conditions on AAEs, the AAEs were plotted against modified combustion efficiencies (MCEs, SI Figure S6). Due to the lack of a sufficient number of coal samples, we only considered the relationships for the crop residues emissions. As shown in SI Figure S6, the AAEs showed a roughly negative correlation with the MCEs (R^2 = 0.31), indicating that less efficient burning phases (smoldering; MCE < 0.9) favor the production of BrC relative to more efficient burning conditions (flaming; MCE > 0.9). Similar negative relationships between these variables also have been reported by Mcmeeking et al. (2015) for emissions from fuels burned in prescribed fires and wildfires and by Pokhrel et al. (2016) for emissions from a variety of globally significant biomass fuels. The dependence of AAEs on MCEs may be attributed to the variations in BrC and BC produced under different combustion conditions. For instance, BrC is preferentially generated during the smoldering phase (low-temperature burning) of combustion (Chakrabarty et al., 2010; Chakrabarty et al., 2014), while BC is mainly emitted during the flaming phase (high-temperature burning) (Bond et al., 2013; Yokelson et al., 1997).

Based on the equations 4 and 5, we calculated the contributions of BrC to the total particles light absorption at different wavelengths from crop residues and bituminous coal emissions (Figure 1). For burning straw or stalks of wheat, corn, rice, soybean, cotton, and sesame, BrC contributed substantially to the total light absorption, which accounted for > 50% in the UV and blue spectral range (370–500 nm). At a wavelength of 370 nm, those contributions were as high as 68–85%. It should be noted that BrC from sugarcane top emissions contributed less to the total light absorption (41%) compared with other crop residues. This may be attributed to the higher MCEs for sugarcane top test burns (SI Figure S6), which are more propitious to producing BC than BrC. In contrast to the biomass burning studies, BrC emitted from hv- and lv-coal combustion tests had lower contributions to the total light absorption under the assumption of AAE_{BC} = 1.0, accounting for only 15% and 18% of the absorption at λ = 370 nm, respectively. The results indicated that BC is the dominant contributor to the particulate absorption in bituminous coal emissions. As discussed in SI Text S1, if one takes into account the uncertainties in AE33 measurements and AAE_{BC} varying from 0.8 to 1.4, the contributions of BrC to the total light absorption at 370 nm have relative uncertainties of [-100%, 108%] for the 15% from hv-coal combustion, and [-100 %, 87%] for the 18% from lv-coal burning, respectively. This indicates BrC emitted from coal burning makes no contribution to the total particles light absorption for higher AAE_{BC} (> 1.2). The higher AAE_{BC} might be caused by BC particles emitted from residential coal burning highly coated in purely scattering material (not BrC) (Lack and Cappa, 2010).

3.2. BrC absorption during the burning process

To investigate real-time emission characteristics of BrC absorption, we plotted the time series of $b_{abs-BrC}$, b_{abs-BC}, and the contribution of BrC to the total light absorption (C_{BrC} = $b_{abs-BrC}/(b_{abs-BrC} + b_{abs-BC})$) in Figure 2(a–d). The data plotted were for at λ = 370 nm, and the

results covered the complete burning cycle of typical crop residues and bituminous coals. Both crop residues and bituminous coals showed unimodal patterns in b_{abs-BC}. There were obvious differences in the emission processes for $b_{abs-BrC}$, however; for the typical crop residues (wheat straw and rice straw), BrC emissions can be roughly divided into three phases (Figure 2a and b). Phase I was the ignition stage. The $b_{abs-BrC}$ increased sharply and showed a peak in C_{BrC} soon after the ignition. The peak in brown carbon emission was short-lived. At the initial stage of heat release, the volatile organic matter (including BrC) was rapidly volatilized during the low-temperature pyrolysis of cellulose, and that led to an increase in BrC absorption. As the devolatilization rate decreased with time, BrC emissions decreased correspondingly. Phase II was the intermediate stage, which was characterized by an enhancement of BrC absorption. During this stage, as the flame intensity and combustion temperature enhanced, the devolatilization rate increased again on the one hand; on the other hand the volatilized organic materials would be burned rapidly at high temperature. The interaction of these two processes resulted in a sharp increase in BrC emissions and the highest $b_{abs-BrC}$ peak. With the continued combustion of crop residues, $b_{abs-BrC}$ decreases gradually. Phase III was the ember combustion stage, and that was characterized by smoldering (MCE < 0.9). During this final stage, volatile materials produced by pyrolysis were almost exhausted, which led to low $b_{abs-BrC}$. As shown in SI Figure S7, other crop residues (corn stalk, soybean straw, cotton stalk, sesame stalk, and sugarcane top) showed emission process similar to those of wheat straw and rice straw.

The BrC emitted from the bituminous coal burning experiments showed different patterns compared with the crop residues burns (Figure 2c and d). The hv- and lv-coal emissions exhibited three similar phases. Phase I was the coal ignition stage, which was characterized by high $b_{abs-BrC}$. During this stage, the incomplete combustion of volatilized matter from coal resulted in large quantities of organic compounds escaping from the combustion region and ultimately leading to high C_{BrC}. Near the end of this stage, $b_{abs-BrC}$ decreased as the escaped devolatilized materials become less. Phase II was the intense combustion stage. During this stage, the coal samples reached the kindling point and volatile compounds began to burn due to the high-temperature flaming combustion. As a result, the $b_{abs-BrC}$ increased again. Because the maximum rate of devolatilization occurred in this stage (Xiao, 2015), a peak in $b_{abs-BrC}$ was found that was higher compared with during the ignition stage; that was true for both types of coal. Although both $b_{abs-BrC}$ and b_{abs-BC} increased during Phase II, C_{BrC} maintained at low values (< 15%), suggesting that BC was the predominant contributor to absorption during this phase. In Phase III, after the intense combustion stage, the coal volatile matters were entirely consumed, and $b_{abs-BrC}$ gradually decreased.

3.3. Absorption emission factors

The calculated absorption emission factors for brown carbon and black carbon (AEF_{BrC} and AEF_{BC}) at different wavelengths from crop residues and bituminous coals are presented in Figure 3. It is evident that the UV-absorption (370 nm) showed the largest AEF_{BrC} for all types of test burns. The AEF_{BrC} decreased as the wavelength increased, with the high goodness of power law fit ($R^2 > 0.88$). For the test burns of crop residues except sugarcane top, the AEF_{BrC} were lower than AEF_{BC} at the wavelength of ~500–880 nm but the reverse was true ($AEF_{BrC} > AEF_{BC}$) at shorter wavelengths (370–500 nm). Given burning same mass of biomass, the BrC absorption emission at short wavelengths was stronger than BC absorption. For the UV-absorption ($\lambda = 370$ nm), the average AEF_{BrC} were 20.9 ± 4.7, 24.2 ± 3.6, 15.2 ± 4.5, 14.3 ± 2.0, 15.8 ± 5.1, and 46.6 ± 16.3 m^2 kg^{-1} for wheat, corn, rice, soybean, cotton, and sesame residues, respectively, with corresponding AEF_{BC} of 5.2 ± 1.2, 4.4 ± 1.2, 5.0 ± 1.6, 7.4 ± 1.1, 5.6 ± 0.6, and 19.2 ± 4.5 m^2 kg^{-1}. The AEF_{BrC} was larger and

significantly different from AEF_{BC} at 95% confidence level (paired t-test, $p < 0.05$). Our results concerning the AEFs are comparable with the values reported by Martinsson et al. (2015) who burned logs of birch and found the AEF_{BrC} and AEF_{BC} for the emissions in the range of 19–24 and 6–7 $m^2 kg^{-1}$ at $\lambda = 370$ nm, respectively. Unlike crop residues emissions, the AEF_{BrC} values for bituminous coals were significant lower (paired t-test, $p < 0.05$) than values of AEF_{BC} at all wavelengths. These differences may be related to fuel properties of coal compared with biomass, and the relatively higher temperatures in the coal burning may have favored the formation of BC. Indeed, a study by Klein et al. (2018) showed a temperature 500–800 °C in the chamber of a traditional household stove that was measured with a thermocouple probe situated closely above the Chinese coal. This is much higher than the pyrolysis temperature of biomass (~210–360 °C) (Li et al., 2016b; White and Dietenberger, 2001). For coal-burning emissions, the AEF_{BrC} (13.64 $\pm$ 0.13 $m^2 kg^{-1}$) and AEF_{BC} (94.79 $\pm$ 15.64 $m^2 kg^{-1}$) for hv-coal were ~6–10 times higher than those for lv-coal (2.01 $\pm$ 0.44 $m^2 kg^{-1}$ for AEF_{BrC} and 9.46 $\pm$ 3.17 $m^2 kg^{-1}$ for AEF_{BC}, respectively). The reason for the observed wide range in AEFs from bituminous coal burning may be related to the higher emissions of carbonaceous aerosol that had high contents of volatile matter (Li et al., 2016a).

3.4. Optical emission inventory

The total ACS_{BrC} emissions from biomass burning and residential coal burning for China in 2015 were estimated to be 4194 Gm^2 (1 $Gm^2 = 10^9 m^2$) and 615 Gm^2, respectively. As shown in Figure 4, the geographic distributions of ACS_{BrC} emissions from burning of biomass and residential coal varied strongly; for example, eastern China had significantly higher ACS_{BrC} emission intensities than western China. For biomass burning (Figure 4a), a hotspot for the ACS_{BrC} emission intensities was the North China Plain (2.67 $Mm^2 km^{-2}$) (1 $Mm^2 = 10^6 m^2$), and the emissions there amounted to 34.7% of the total ACS_{BrC} emission for China. The Lianghu Plain (Hubei and Hunan Provinces) and Sichuan Basin had more moderate emission intensities (1.38 and 0.78 $Mm^2 km^{-2}$, respectively). The regions with high ACS_{BrC} emission intensities are major crop producing areas, and they are not only characterized by extensive cultivated areas but also by their dense populations. Indeed, greater agricultural and rural activities have been linked to the high emissions (Zhou et al., 2017). It is noteworthy that several areas in Guangxi and Guangdong Provinces also had substantial ACS_{BrC} emission intensity (0.99 $Mm^2 km^{-2}$). This can be explained by the fact that > 80% of the sugarcane top burning in China occurs in those two provinces. Another important agricultural zone, Northeast China showed a relatively low intensity (0.55 $Mm^2 km^{-2}$) due to its large area. The most regions with the lowest emission intensities (< 0.1 $Mm^2 km^{-2}$) were concentrated in Qinghai, Tibet, and Xinjiang Provinces.

Biomass is traditionally burned in the field, and the burning mainly occurs before the crop sowing and after the harvest season. A seasonal breakdown of the ACS_{BrC} emission intensities from biomass burned in the field shows obvious differences in the temporal variations among the regions (SI Figure S8). For the major agricultural zones in the northern plain of China (zone 1, SI Figure S1a), the high ACS_{BrC} emission intensity was found in summer, and that pattern is in general agreement with agricultural cycles of summer corn (planted in June and harvested in September) and winter wheat (sown in October and reaped in May). The northeast region (zone 2) showed high values in spring when the fields are burned prior to the planting of spring corn (April) and bean (mid-May) and in autumn, which is presumably due to the fall harvest beginning in the early October. Planting in zone 3 (southern China) starts earlier than the norther parts of China, and as a result, the high

ACS$_{BrC}$ emission intensity occurs in spring. In this zone, the late rice crop successively mature in November that causes the high value in winter (Huang et al., 2012).

The spatial distribution of ACS$_{BrC}$ emissions for residential coal burning was different from that for biomass burning (Figure 4b). The highest ACS$_{BrC}$ emission area was situated in the Beijing-Tianjin-Hebei region (0.56 Mm^2 km^{-2}), where accounted for > 20% of national ACS$_{BrC}$ emissions in China from residential coal burning. The heavy use of coal for residential heating and cooking in this region was concluded to be the major contributor to local air pollution during the wintertime (Zhang et al., 2017). Shanxi (0.36 Mm^2 km^{-2}) and Guizhou (0.28 Mm^2 km^{-2}) Provinces also showed substantial ACS$_{BrC}$ emissions because they are major coal-producing regions, and people in rural parts of those provinces can purchase coal at lower price than other regions in China. In addition to the high ACS$_{BrC}$ emission from biomass burning, the impact from coal burning was also substantial in Henan Province (0.25 Mm^2 km^{-2}), that was possibly related to a higher space heating demand in winter due to its large rural population and area. Lower ACS$_{BrC}$ emission intensities (< 0.05 Mm^2 km^{-2}) were mainly distributed in southern China (including Guangxi, Guangdong, Fujian, and Hainan Provinces) where the climate is warm and in northwest China where the provinces (including Xinjiang, Inner Mongolia, and Qinghai Provinces) are large in area and sparse in population.

The uncertainties in ACS$_{BrC}$ emissions from burning of biomass and residential coal were quantitatively evaluated through Monte Carlo simulations, which have been used for this purpose in mass emission inventories (Qin and Xie, 2011; Wang et al., 2012; Yan et al., 2006). The probability distributions of biomass and residential coal consumption were assumed to be normal, and coefficients of variation (CV, the standard deviation divides by the mean) were set at 30% and 20%, respectively, based on results in Zhao et al. (2011). The assumption that probability distributions of AEFs were lognormal follows the work of Bond et al. (2004), and the CVs (logarithmic standard deviation divides by the logarithmic mean) were 2–14% and 3–32% for burning of crop residues and residential coals, respectively. Finally, the CVs of activity data and the AEFs and their corresponding statistical distributions were used as the input data for Monte Carlo analysis, and 100,000 simulations were performed to estimate the uncertainties. The probability distributions of ACS$_{BrC}$ emissions for burning of biomass and residential coals are shown in Figure 5. The values of mean, 2.5th percentile, and 97.5th percentile were 4224, 2823, and 5966 Gm^2 for biomass burning and 614, 373, and 860 Gm^2 for residential coal combustion. The overall uncertainties at the 95% confidence interval for ACS$_{BrC}$ emissions were -33.2 to 41.2% for biomass burning and -39.3 to 40.1% for residential coal combustion. A follow-up analyses showed that the activity data including the mass of biomass and residential coal burned in China changed slightly between the year of 2015 and 2016 (SI Figure S9), and that resulted in similar emissions of ACS$_{BrC}$ (SI Figure S10).

4. Conclusion

The real-time light-absorbing characteristics of BrC from biomass and coal burning were investigated through a series of laboratory experiments. The AAEs for the wavelength pair of 370 and 880 nm ranged from 1.19 to 3.25, suggesting the possible existence of BrC in both biomass- and coal-burning emissions. Based on the assumption that AAE$_{BC}$ = 1.0, BrC from biomass burning contributed to 41–85% of the total light absorption at 370 nm, whereas that from burning of bituminous coal only accounted for 15–18%. Moreover, a roughly negative correlation (R^2 = 0.31) between AAEs and modified combustion efficiencies was found for the biomass-burning experiments. The AEF$_{BrC}$ values at λ = 370 nm were estimated to be 15–47 m^2 kg^{-1} for biomass and 2–13 m^2 kg^{-1} for bituminous coal, respectively. Based on

those AEF$_{BrC}$ results and county-level activity data, high-resolution optical emission inventories of BrC were developed for China in 2015. The estimated total annual ACS$_{BrC}$ emissions from biomass and residential coal burning were 4194 Gm^2 (-33.2, 41.2%) and 615 Gm^2 (-39.3, 40.1%), respectively. High ACS$_{BrC}$ emission intensities from biomass-burning emission were mainly found in the North China Plain (Shandong, Henan, Anhui, and Jiangsu Provinces) (2.67 Mm^2 km^{-2}), Lianghu Plain (Hubei, and Hunan Provinces) (1.38 Mm^2 km^{-2}) and Sichuan Basin (0.78 Mm^2 km^{-2}), which are the important agricultural zones. The highest ACS$_{BrC}$ intensity from coal-burning emission was found in the Beijing-Tianjin-Hebei region, presumably due to the large space heating demand in the wintertime. To the best of our knowledge, this is the first data set that provides an optical emission inventory for BrC in China, and the results could be used in models to assess the radiative effects of BrC.

Acknowledgments

References

Andreae, M. O., & Gelencsér, A. (2006). Black carbon or brown carbon? The nature of light-absorbing carbonaceous aerosols. *Atmospheric Chemistry and Physics*, *6*(10), 3131-3148. https://doi.org/10.5194/acp-6-3131-2006

Bahadur, R., Praveen, P. S., Xu, Y., & Ramanathan, V. (2012). Solar absorption by elemental and brown carbon determined from spectral observations. *Proceedings of the National Academy of Sciences of the United States of America*, *109*(43), 17366-17371. https://doi.org/10.1073/pnas.1205910109

Bergstrom, R. W., Russell, P. B., & Hignett, P. (2002). Wavelength dependence of the absorption of black carbon particles: Predictions and results from the TARFOX experiment and implications for the aerosol single scattering albedo. *Journal of the Atmospheric Sciences*, *59*(3), 567-577. https://doi.org/10.1175/1520-0469(2002)059<0567:WDOTAO>2.0.CO;2

Bond, T. C., Doherty, S. J., Fahey, D. W., Forster, P. M., Berntsen, T., DeAngelo, B. J., Flanner, M. G., Ghan, S., Karcher, B., Koch, D., Kinne, S., Kondo, Y., Quinn, P. K., Sarofim, M. C., Schultz, M. G., Schulz, M., Venkataraman, C., Zhang, H., Zhang, S., Bellouin, N., Guttikunda, S. K., Hopke, P. K., Jacobson, M. Z., Kaiser, J. W., Klimont, Z., Lohmann, U., Schwarz, J. P., Shindell, D., Storelvmo, T., Warren, S. G., & Zender, C. S. (2013). Bounding the role of black carbon in the climate system: A scientific assessment. *Journal of Geophysical Research: Atmospheres*, *118*, 5380-5552. https://doi.org/10.1002/jgrd.50171

Bond, T. C., & Bergstrom, R. W. (2006). Light absorption by carbonaceous particles: An investigative review. *Aerosol Science and Technology*, *40*(1), 27-67. https://doi.org/10.1080/02786820500421521

Bond, T. C., Streets, D. G., Yarber, K. F., Nelson, S. M., Woo, J.-H., & Klimont, Z. (2004). A technology-based global inventory of black and organic carbon emissions from

combustion. *Journal of Geophysical Research: Atmospheres*, *109*(D14), D14203. https://doi.org/10.1029/2003JD003697

Chakrabarty, R. K., Moosmüller, H., Chen, L.-W. A., Lewis, K., Arnott, W. P., Mazzoleni, C., Dubey, M. K., Wold, C. E., Hao, W. M., & Kreidenweis, S. M. (2010). Brown carbon in tar balls from smoldering biomass combustion. *Atmospheric Chemistry and Physics*, *10*(13), 6363-6370. https://doi.org/10.5194/acp-10-6363-2010

Chakrabarty, R. K., Pervez, S., Chow, J. C., Watson, J. G., Dewangan, S., Robles, J., & Tian, G. (2014). Funeral pyres in South Asia: Brown carbon aerosol emissions and climate impacts. *Environmental Science & Technology Letters*, *1*(1), 44-48. https://doi.org/10.1021/ez4000669

Chang, M. O., Chow, J. C., Watson, J. G., Hopke, P. K., Yi, S. M., & England, G. C. (2004). Measurement of ultrafine particle size distributions from coal-, oil-, and gas-fired stationary combustion sources. *Journal of the Air & Waste Management Association*, *54*(12), 1494-1505. https://doi.org/10.1080/10473289.2004.10471010

Chen, Y., & Bond, T. C. (2010). Light absorption by organic carbon from wood combustion. *Atmospheric Chemistry and Physics*, *10*(4), 1773-1787. https://doi.org/10.5194/acp-10-1773-2010

Cheng, Y., He, K. B., Zheng, M., Duan, F. K., Du, Z. Y., Ma, Y. L., Tan, J. H., Yang, F. M., Liu, J. M., Zhang, X. L., Weber, R. J., Bergin, M. H., & Russell, A. G. (2011). Mass absorption efficiency of elemental carbon and water-soluble organic carbon in Beijing, China. *Atmospheric Chemistry and Physics*, *11*(22), 11497-11510. https://doi.org/10.5194/acp-11-11497-2011

Chow, J. C., Watson, J. G., Lowenthal, D. H., Chen, L.-W. A., & Motallebi, N. (2010). Black and organic carbon emission inventories: Review and application to California. *Journal of the Air & Waste Management Association*, *60*(4), 497-507. https://doi.org/10.3155/1047-3289.60.4.497

Chung, C. E., Ramanathan, V., & Decremer, D. (2012). Observationally constrained estimates of carbonaceous aerosol radiative forcing. *Proceedings of the National Academy of Sciences of the United States of America*, *119*(29), 11624-11629. https://doi.org/10.1073/pnas.1203707109

Clarke, A., McNaughton, C., Kapustin, V., Shinozuka, Y., Howell, S., Dibb, J., Zhou, B., Anderson, B., Brekhovskikh, V., Turner, H., & Pinkerton, M. (2007). Biomass burning and pollution aerosol over North America: Organic components and their influence on spectral optical properties and humidification response. *Journal of Geophysical Research: Atmospheres*, *112*, D12S18. https://doi.org/10.1029/2006JD007777

De Haan, D. O., Hawkins, L. N., Kononenko, J. A., Turley, J. J., Corrigan, A. L., Tolbert, M. A., & Jimenez, J. L. (2011). Formation of nitrogen-containing oligomers by methylglyoxal and amines in simulated evaporating cloud droplets. *Environmental Science & Technology*, *45*(3), 984-991. https://doi.org/10.1021/es102933x

Drinovec, L., Močnik, G., Zotter, P., Prévôt, A., Ruckstuhl, C., Coz, E., Rupakheti, M., Sciare, J., Müller, T., Wiedensohler, A., & Hansen, A. D. A. (2015). The "dual-spot" Aethalometer: an improved measurement of aerosol black carbon with real-time loading compensation. *Atmospheric Measurement Techniques*, *8*(5), 1965-1979. https://doi.org/10.5194/amt-8-1965-2015

Feng, Y., Ramanathan, V., & Kotamarthi, V. R. (2013). Brown carbon: a significant atmospheric absorber of solar radiation? *Atmospheric Chemistry and Physics*, *13*(17), 8607-8621. https://doi.org/10.5194/acp-13-8607-2013

Forrister, H., Liu, J., Scheuer, E., Dibb, J., Ziemba, L., Thornhill, K. L., Anderson, B., Diskin, G., Perring, A. E., Schwarz, J. P., Campuzano-Jost, P., Day, D. A., Palm, B. B., Jimenez, J. L., Nenes, A., & Weber, R. J. (2015). Evolution of brown carbon in wildfire plumes.

Geophysical   Research   Letters,   *42*(11),   4623-4630. https://doi.org/10.1002/2015GL063897

Fu, T.-M., Cao, J. J., Zhang, X. Y., Lee, S. C., Zhang, Q., Han, Y. M., Qu, W. J., Han, Z., Zhang, R., Wang, Y. X., Chen, D., & Henze, D. K. (2012). Carbonaceous aerosols in China: top-down constraints on primary sources and estimation of secondary contribution. *Atmospheric   Chemistry   and   Physics*, *12*(5),   2725-2746. https://doi.org/10.5194/acp-12-2725-2012

Hecobian, A., Zhang, X., Zheng, M., Frank, N., Edgerton, E. S., & Weber, R. J. (2010). Water-Soluble Organic Aerosol material and the light-absorption characteristics of aqueous extracts measured over the Southeastern United States. *Atmospheric Chemistry and Physics*, *10*, 5965-5977. https://doi.org/10.5194/acp-10-2965-2010

Hoffer, A., Gelenscér, A., Guyon, P., Kiss, G., Schmid, O., Frank, G. P., Artaxo, P., & Andreae, M. O. (2006). Optical properties of humic-like substances (HULIS) in biomass-burning aerosols. *Atmospheric Chemistry and Physics*, *6*, 3563-3570. https://doi.org/10.5194/acpd-5-7341-2005

Huang, X., Song, Y., Li, M., Li, J., & Zhu, T. (2012). Harvest season, high polluted season in East   China.   *Environmental   Research   Letters*,   *7*(4),   044033. https://doi.org/10.1088/1748-9326/7/4/044033

IPCC. (2013). Climate Change 2013: The Physical Science Basis. Contribution of Working Group I to the Fifth Assessment Reprot of the Intergovemental Panel on Climate Change [Stocker, T.F., D. Qin, G.-K. Plattner, M. Tignor, S.K. Allen, J. Boschung, A. Nauels, Y. Xia, V. Bex and P.M. Midgley (eds.)]. *Cambridage University Press, Cambrigde, United Kingdom and New York, NY, USA*, *1535pp*.

Jo, D. S., Park, R. J., Lee, S., Kim, S. W., & Zhang, X. (2016). A global simulation of brown carbon: Implications for photochemistry and direct radiative effect. *Atmospheric Chemistry and Physics*, *15*(19), 27805-27852. https://doi.org/10.5194/acp-16-3413-2016

Kirchstetter, T. W., Novakov, T., & Hobbs, P. V. (2004). Evidence that the spectral dependence of light absorption by aerosols is affected by organic carbon. *Journal of Geophysical   Research: Atmospheres*,   *109*,   D21208. https://doi.org/10.1029/2004JD004999

Kirchstetter, T. W., & Thatcher, T. L. (2012). Contribution of organic carbon to wood smoke particulate matter absorption of solar radiation. *Atmospheric Chemistry and Physics*, *12*, 6067-6072. https://doi.org/10.5194/acp-12-6067-2012

Kirillova, E. N., Andersson, A., Han, J., Lee, M., & Gustafsson, Ö. (2014). Sources and light absorption of water-soluble organic carbon aerosols in the outflow from northern China. *Atmospheric Chemistry and Physics*, *14*(3), 1413-1422. https://doi.org/10.5194/acp-14-1413-2014

Klein, F., Pieber, S. M., Ni, H., Stefenelli, G., Bertrand, A., Kilic, D., Pospisilova, V., Temime-Roussel, B., Marchand, N., El Haddad, I., Slowik, J. G., Baltensperger, U., Cao, J., Huang, R., & Prévôt, A. S. H. (2018). Characterization of Gas-phase organics using proton transfer reaction time-of-flight mass spectrometry: Residential coal combustion. *Environmental   Science   &   Technology*,   *52*(5),   2612-2617. https://doi.org/10.1021/acs.est.7b03960

Koch, D., Bond, T. C., Streets, D., Unger, N., & van der Werf, G. R. (2007). Global impacts of aerosols from particular source regions and sectors. *Journal of Geophysical Research: Atmospheres*, *112*, D02205. https://doi.org/10.1029/2005JD007024

Lack, D. A., & Langridge, J. M. (2013). On the attribution of black and brown carbon light absorption using the Ångström exponent. *Atmospheric Chemistry and Physics*, *13*(20), 10535-10543. https://doi.org/10.5194/acp-13-10535-2013

Lack, D. A., Bahreini, R., Langridge, J. M., Gilman, J. B., & Middlebrook, A. M. (2013). Brown carbon absorption linked to organic mass tracers in biomass burning particles. *Atmospheric Chemistry and Physics*, *13*(5), 2415-2422. https://doi.org/ 10.5194/acp-13-2415-2013

Lack, D. A., & Cappa, C. D. (2010). Impact of brown and clear carbon on light absorption enhancement, single scatter albedo and absorption wavelength dependence of black carbon. *Atmospheric Chemistry and Physics*, *10*, 4207-4220. https://doi.org/10.5194/acp-10-4207-2010

Laing, J. R., Jaffe, D. A., & Hee, J. R. (2016). Physical and optical properties of aged biomass burning aerosol from wildfires in Siberia and the Western USA at the Mt. Bachelor Observatory. *Atmospheric Chemistry and Physics*, *16*, 15185-15197. https://doi.org/10.5194/acp-16-15185-2016

Laskin, J., Laskin, A., Nizkorodov, S. A., Roach, P., Eckert, P., Gilles, M. K., Wang, B. B., Lee, H. J., & Hu, Q. C. (2014). Molecular selectivity of brown carbon chromophores. *Environmental Science & Technology*, *48*(20), 12047-12055. https://doi.org/10.1021/es503432r

Li, N., Fu, T. M., Cao, J. J., Lee, S. C., Huang, X. F., He, L. Y., Ho, K. F., Fu, J. S., & Lam, Y. F. (2013). Sources of secondary organic aerosols in the Pearl River Delta region in fall: Contributions from the aqueous reactive uptake of dicarbonyls. *Atmospheric Environment*, *76*(3), 200-207. https://doi.org/10.1016/j.atmosenv.2012.12.005

Li, Q., Jiang, J., Zhang, Q., Zhou, W., Cai, S., Duan, L., Ge, S., & Hao, J. (2016a). Influences of coal size, volatile matter content, and additive on primary particulate matter emissions from household stove combustion. *Fuel*, *182*, 780-787. https://doi.org/10.1016/j.fuel.2016.06.059

Li, X., Chen, Y., & Bond, T. C. (2016b). Light absorption of organic aerosol from pyrolysis of corn stalk. *Atmospheric Environment*, *144*, 249-256. https://doi.org/10.1016/j.atmosenv.2016.09.006

Li, X., Wang, S., Duan, L., Hao, & Long, Z. (2011). Design of a compact dilution sampler for stationary combustion sources. *Journal of the Air & Waste Management Association*, *61*, 1124-1130. https://doi.org/10.1080/10473289.2011.604556

Li, X., Duan, L., Wang, S., Duan, J., Guo, X., Yi, H., Hu, J., Li, C & Hao, J. (2007). Emission characteristics of particulate matter from rural household biofuel combustion in China. *Energy & Fuel*, *21*(2), 845-851. https://doi.org/ 10.1021/ef060150g

Lin, G., Penner, J. E., Flanner, M. G., Sillman, S., Xu, L., & Zhou, C. (2014). Radiative forcing of organic aerosol in the atmosphere and on snow: Effects of SOA and brown carbon. *Journal of Geophysical Research: Atmospheres*, *119*(12), 7453-7476. https://doi.org/10.1002/2013JD021186

Lin, P., Laskin, J., Nizkorodov, S. A., & Laskin, A. (2015). Revealing brown carbon chromophores produced in reactions of methylglyoxal with ammonium sulfate. *Environmental Science & Technology*, *49*(24), 14257-14266. https://doi.org/10.1021/acs.est.5b03608

Lipsky, E. M., & Robinson, A. L. (2006). Effects of dilution on fine particle mass and partitioning of semivolatile organics in diesel exhaust and wood smoke. *Environmental Science & Technology*, *40*, 155-162. https://doi.org/10.1021/es050319p

Lipsky, E. M., & Robinson, A. L. (2005). Design and evaluation of a portable dilution sampling system for measuring fine particle emissions. *Aerosol Science and Technology*, *39*(6), 542-553. https://doi.org/10.1080/027868291004850

Lu, Z., Streets, D. G., Winijkul, E., Yan, F., Chen, Y., Bond, T. C., Feng, Y., Dubey, M. K., Liu, S., Pinto, J. P., & Carmichael, G. R. (2015). Light absorption properties and

radiative effects of primary organic aerosol emissions. *Environmental Science & Technology*, *49*(8), 4868-4877. https://doi.org/10.1021/acs.est.5b00211

Martinsson, J., Eriksson, A. C., Nielsen, I. E., Malmborg, V. B., Ahlberg, E., Andersen, C., Lindgren, R., Nyström, R., Nordin, E. Z., Brune, W. H., Svenningsson, B., Swietlicki, E., Boman, C., & Pagels, J. H. (2015). Impacts of combustion conditions and photochemical processing on the light absorption of biomass combustion aerosol. *Environmental Science & Technology*, *49*(24), 14663-14671. https://doi.org/10.1021/acs.est.5b03205

Mcmeeking, G. R., Fortner, E., Onasch, T. B., Taylor, J. W., Flynn, M., Coe, H., & Kreidenweis, S. M. (2015). Impacts of nonrefractory material on light absorption by aerosols emitted from biomass burning. *Journal of Geophysical Research: Atmospheres*, *119*(21), 12,272-212,286. https://doi.org/10.1002/2014JD021750

Moosmüller, H., Chakrabarty, R. K., Ehlers, K. M., & Arnott, W. P. (2011). Absorption Ångström coefficient, brown carbon, and aerosols: basic concepts, bulk matter, and spherical particles. *Atmospheric Chemistry and Physics*, *11*, 1217-1225. https://doi.org/10.5194/acp-11-1217-2011

Myhre, G., Hoyle, C. R., Berglen, T. F., Johnson, B. T., & Haywood, J. M. (2008). Modeling of the solar radiative impact of biomass burning aerosols during the Dust and Biomass-burning Experiment (DABEX). *Journal of Geophysical Research: Atmospheres*, *113*, D00C16. https://doi.org/10.1029/2008JD009857

Nakayama, T., Ikeda, Y., Sawada, Y., Setoguchi, Y., Ogawa, S., Kawana, K., Mochida, M., Ikemori, F., Matsumoto, K., & Matsumi, Y. (2014). Properties of light-absorbing aerosols in the Nagoya urban area, Japan, in August 2011 and January 2012: Contributions of brown carbon and lensing effect,. *Journal of Geophysical Research: Atmospheres*, *119*, 12721-12739. https://doi.org/10.1002/2014JD021744

National Bureau of Statistics of the People's Republic of China (NBS). (2016a). China Statistical Yearbook (2016). *China Statistics Press* (in Chinese).

National Bureau of Statistics of the People's Republic of China (NBS). (2016b). China Energy Statistical Yearbook (2016). *China Statistics Press* (in Chinese).

Nguyen, T. B., Lee, P. B., Updyke, K. M., Bones, D. L., Laskin, J., Laskin, A., & Nizkorodov, S. A. (2012). Formation of nitrogen- and sulfur-containing light-absorbing compounds accelerated by evaporation of water from secondary organic aerosols. *Journal of Geophysical Research: Atmospheres*, *117*, D01207. https://doi.org/10.1029/2011JD016944

Ni, H., Han, Y., Cao, J., Chen, L.-W. A., Tian, J., Wang, X., Chow, J. C., Watson, J. G., Wang, Q., Wang, P., Li, H., & Huang, R. (2015). Emission characteristics of carbonaceous particles and trace gases from open burning of crop residues in China. *Atmospheric Environment*, *123*, 399-406. https://doi.org/10.1016/j.atmosenv.2015.05.007

Nozière, B., Dziedzic, P., & Córdova, A. (2007). Formation of secondary light-absorbing "fulvic-like" oligomers: A common process in aqueous and ionic atmospheric particles? *Geophysical Research Letters*, *34*(21), L21812. https://doi.org/ 10.1029/2007GL031300

Olson, M. R., Garcia, M. V., Robinson, M. A., Rooy, P. V., Dietenberger, M. A., Bergin, M., & Schauer, J. J. (2015). Investigation of black and brown carbon multiple-wavelength-dependent light absorption from biomass and fossil fuel combustion source emissions. *Journal of Geophysical Research: Atmospheres*, *120*, 6682-6697. https://doi.org/10.1002/2014JD022970

Pandey, A., Pervez, S., & Chakrabarty, R. K. (2016). Filter-based measurements of UV–vis mass absorption cross sections of organic carbon aerosol from residential biomass combustion: Preliminary findings and sources of uncertainty. *Journal of Quantitative*

Spectroscopy & Radiative Transfer, *182*, 296-304. https://doi.org/10.1016/j.jqsrt.2016.06.023

Pokhrel, R. P., Beamesderfer, E. R., Wagner, N. L., Langridge, J. M., Lack, D. A., Jayarathne, T., Stone, E. A., Stockwell, C. E., Yokelson, R. J., & Murphy, S. M. (2017). Relative importance of black carbon, brown carbon and absorption enhancement from clear coatings in biomass burning emissions. *Atmospheric Chemistry and Physics*, *17*(8), 5063-5078. https://doi.org/10.5194/acp-17-5063-2017

Pokhrel, R. P., Wagner, N. L., Langridge, J. M., Lack, D. A., Jayarathne, T., Stone, E. A., Stockwell, C. E., Yokelson, R. J., & Murphy, S. M. (2016). Parameterization of single-scattering albedo (SSA) and absorption Ångström exponent (AAE) with EC/OC for aerosol emissions from biomass burning. *Atmospheric Chemistry and Physics*, *16*(15), 9549-9561. https://doi.org/10.5194/acp-16-9549-2016

Powelson, M. H., Espelien, B. M., Hawkins, L. N., Galloway, M. M., & De Haan, D. O. (2014). Brown carbon formation by aqueous-phase carbonyl compound reactions with amines and ammonium sulfate. *Environmental Science & Technology*, *48*(2), 985-993. https://doi.org/ 10.1021/es4038325

Qin, Y., & Xie, S. (2011). Estimation of county-level black carbon emissions and its spatial distribution in China in 2000. *Atmospheric Environment*, *45*(38), 6995-7004. https://doi.org/10.1016/j.atmosenv.2011.09.017

Saleh, R., Marks, M., Heo, J., Adams, P. J., Donahue, N. M., & Robinson, A. L. (2015). Contribution of brown carbon and lensing to the direct radiative effect of carbonaceous aerosols from biomass and biofuel burning emissions. *Journal of Geophysical Research: Atmospheres*, *120*(19), 10285-10296. https://doi.org/10.1002/2015JD023697

Saleh, R., Hennigan, C. J., McMeeking, G. R., Chuang, W. K., Robinson, E. S., Coe, H., Donahue., N. M., & Robinson, A. L. (2013). Absorptivity of brown carbon in fresh and photo-chemically aged biomass-burning emissions. *Atmospheric Chemistry and Physics*, *13*(15), 7683-7693. https://doi.org/10.5194/acp-13-7683-2013

Schnaiter, M., Gimmler, M., Llamas, I., Linke, C., Ger, C. J., & Mutschke, H. (2006). Strong spectral dependence of light absorption by organic carbon particles formed by propane combustion. *Atmospheric Chemistry and Physics*, *6*(10), 2981-2990. https://doi.org/10.5194/acp-6-2981-2006

Shen, Z. X., Zhang, Q., Cao, J. J., Zhang, L. M., Lei, Y. L., Huang, Y., Huang, R. J., Gao, J. J., Zhao, Z. Z., Zhu, C. S., Yin, X., Zheng, C. L., Xu, H. M., & Liu, S. X. (2016). Optical properties and possible sources of brown carbon in $PM_{2.5}$ over Xi'an, China. *Atmospheric Environment*, *150*, 322-330. https://doi.org/10.1016/j.atmosenv.2016.11.024

Srinivas, B., & Sarin, M. M. (2014). Brown carbon in atmospheric outflow from the Indo-Gangetic Plain: Mass absorption efficiency and temporal variability. *Atmospheric Environment*, *89*(2), 835-843. https://doi.org/10.1016/j.atmosenv.2014.03.030

Sun, H., Biedermann, L., & Bond, T. C. (2007). Color of brown carbon: A model for ultraviolet and visible light absorption by organic carbon aerosol. *Geophysical Research Letters*, *34*(17), 251-270. https://doi.org/10.1029/2007GL029797

Sun, J., Zhi, G., Hitzenberger, R., Chen, Y., Tian, C., Zhang, Y., Feng, Y., Cheng, M., Zhang, Y., Cai, J., Chen, F., Qiu, Y., Jiang, Z., Li, J., Zhang, G., & Mo, Y. (2017). Emission factors and light absorption properties of brown carbon from household coal combustion in China. *Atmospheric Chemistry and Physics*, *17*(7), 4769-4780. https://doi.org/10.5194/acp-17-4769-2017

Tian, J., Chow, J. C., Cao, J., Han, Y., Ni, H., Chen, L.-W. A., Wang, X., Huang, R., Moosmüller, H., & Watson, J. G. (2015). A biomass combustion chamber: Design,

evaluation, and a case study of wheat straw combustion emission tests. *Aerosol and Air Quality Research*, *15*, 2104-2114. https://doi.org/10.4209/aaqr.2015.03.0167

Tian, J., Ni, H., Cao, J., Han, Y., Wang, Q., Wang, X., Chen, L.-W. A., Chow, J. C., Watson, J. G., Wei, C., Sun, J., Zhang, T., & Huang, R. (2017). Characteristics of carbonaceous particles from residential coal combustion and agricultural biomass burning in China. *Atmospheric Pollution Research*, *8*(3), 521-527. https://doi.org/10.1016/j.apr.2016.12.006

Titos, G., Lyamani, H., Drinovec, L., Olmo, F. J., Močnik, G., & Alados-Arboledas, L. (2015). Evaluation of the impact of transportation changes on air quality. *Atmospheric Environment*, *114*, 19-31. https://doi.org/10.1016/j.atmosenv.2015.05.027

Utry, N., Ajtai, T., Filep, Á., Pintér, M., Török, Z., Bozóki, Z., & Szabó, G. (2014). Correlations between absorption Angström exponent (AAE) of wintertime ambient urban aerosol and its physical and chemical properties. *Atmospheric Environment*, *91*, 52-59. https://doi.org/10.1016/j.atmosenv.2014.03.047

Wang, R., Tao, S., Wang, W., Liu, J., Shen, H., Shen, G., Wang, B., Liu, X., Li, W., Huang, Y., Zhang, Y., Lu, Y., Chen, H., Chen, Y., Wang, C., Zhu, D., Wang, X., Li, B., Liu, W., & Ma, J. (2012). Black carbon emissions in China from 1949 to 2050. *Environmental Science & Technology*, *46*(14), 7595-7603. https://doi.org/10.1021/es3003684

Wang, X., Heald, C. L., Ridley, D. A., Schwarz, J. P., Spackman, J. R., Perring, A. E., Coe, H., Liu, D., & Clarke, A. D. (2014). Exploiting simultaneous observational constraints on mass and absorption to estimate the global direct radiative forcing of black carbon and brown carbon. *Atmospheric Chemistry and Physics*, *14*(20), 17527-17583. https://doi.org/10.5194/acp-14-10989-2014

Washenfelder, R. A., Attwood, A. R., Brock, C. A., Guo, H., Xu, L., Weber, R. J., Ng, N. L., Allen, H. M., Ayres, B. R., Baumann, K., Cohen, R. C., Draper, D. C., Duffey, K. C., Edgerton, E., Fry, J. L., Hu, W. W., Jimenez, J. L., Palm, B. B., Romer, P., Stone, E. A., Wooldridge, P. J., & Brown, S. S. (2015). Biomass burning dominates brown carbon absorption in the rural southeastern United States. *Geophysical Research Letters*, *42*(2), 653-664. https://doi.org/10.1002/2014GL062444

Weingartner, E., Saathoff, H., Schnaiter, M., Streit, N., Bitnar, B., & Baltensperger, U. (2003). Absorption of light by soot particles: determination of the absorption coefficient by means of aethalometers. *Journal of Aerosol Science*, *34*(10), 1445-1463. https://doi.org/10.1016/S0021-8502(03)00359-8

White, R., & Dietenberger, M. (2001). Wood products: Thermal degradation and fire. *Encyclopedia of Materials: Science and Technology*, 9712-9716. https://doi.org/10.1016/B0-08-043152-6/01763-0

Wonaschütz, A., Hitzenberger, R., Bauer, H., Pouresmaeil, P., Klatzer, B., Caseiro, A., & Puxbaum, H. (2009). Application of the integrating sphere method to separate the contributions of brown and black carbon in atmospheric aerosols. *Environmental Science & Technology*, *43*(4), 1141-1146. https://doi.org/10.1021/es8008503

Xiao, C. W. (2015). Research on combustion features of medium volatile matter bituminous coal. *Coal Science and Technology*, *43*(5), 135-138 (in Chinese). https://doi.org/10.13199/j.cnki.cst.2015.05.033

Yan, C. Q., Zheng, M., Bosch, C., Andersson, A., Desyaterik, Y., Sullivan, A. P., Collett, J. L., Zhao, B., Wang, S .X., He, K. B., & Gustafsson, Ö. (2017). Important fossil source contribution to brown carbon in Beijing during winter. *Scientific Reports*, *7*, 43182. https://doi.org/ 10.1038/srep43182

Yan, X., Ohara, T., & Akimoto, H. (2006). Bottom-up estimate of biomass burning in mainland China. *Atmospheric Environment*, *40*(27), 5262-5273. https://doi.org/10.1016/j.atmosenv.2006.04.040

Yao, H., Song, Y., Liu, M., Archer-Nicholls, S., Lowe, D., McFiggans, G., Xu, T., Du, P., Li, J., Wu, Y., Hu, M., Zhao, C., & Zhu, T. (2017). Direct radiative effect of carbonaceous aerosols from crop residue burning during the summer harvest season in East China. *Atmospheric Chemistry and Physics*, *17*(8), 5205-5219. https://doi.org/10.5194/acp-17-5205-2017

Yokelson, R. J., Susott, R., Ward, D. E., Reardon, J., & Griffith, D. W. (1997). Emissions from smoldering combustion of biomass measured by open-path Fourier transform infrared spectroscopy. *Journal of Geophysical Research: Atmospheres*, *102*(D15), 18865-18877. https://doi.org/10.1029/97JD00852

Zhang, F., Wang, J., Ichoku, C., Hyer, E. J., Yang, Z., Ge, C., Su, S., Zhang, X., Kondragunta, S., & Kaiser, J. W. (2014). Sensitivity of mesoscale modeling of smoke direct radiative effect to the emission inventory: a case study in northern sub-Saharan African region. *Environmental Research Letters*, *9*(7), 075002. https://doi.org/10.1088/1748-9326/9/7/075002

Zhang, Q., Streets, D. G., Carmichael, G. R., He, K. B., Huo, H., Kannari, A., Klimont, Z., Park, I. S., Reddy, S., Fu, J. S., Chen, D., Duan, L., Lei, Y., Wang, L. T., & Yao, Z. L. (2009). Asian emissions in 2006 for the NASA INTEX-B mission. *Atmospheric Chemistry and Physics*, *9*(14), 5131-5153. https://doi.org/10.5194/acp-9-5131-2009

Zhang, X., Lin, Y. H., Surratt, J. D., Zotter, P., Prévôt, A. S. H., & Webber, R .J. (2011). Light‐absorbing soluble organic aerosol in Los Angeles and Atlanta: A contrast in secondary organic aerosol. *Geophysical Research Letters*, *38*(21), 759-775. https://doi.org/10.1029/2011GL049385

Zhang, X., Lin, Y. H., Surratt, J. D., & Weber, R. J. (2013). Sources, composition and Absorption Ångström Exponent of light-absorbing organic components in aerosol extracts from the Los Angeles Basin. *Environmental Science & Technology*, *47*(8), 3685-3693. https://doi.org/10.1021/es305047b

Zhang, Z., Wang, W., Cheng, M., Liu, S., Xu, J., He, Y., & Meng, F. (2017). The contribution of residential coal combustion to $PM_{2.5}$ pollution over China's Beijing-Tianjin-Hebei region in winter. *Atmospheric Environment*, *159*, 147-161. https://doi.org/10.1016/j.atmosenv.2017.03.054

Zhao, Y., Nielsen, C. P., Lei, Y., Mcelroy, M. B., & Hao, J. (2011). Quantifying the uncertainties of a bottom-up emission inventory of anthropogenic atmospheric pollutants in China. *Atmospheric Chemistry and Physics*, *11*(5), 2295-2308. https://doi.org/10.5194/acp-11-2295-2011

Zhou, Y., Xing, X., Lang, J., Chen, D., Cheng, S., Wei, L., Wei, X., & Liu, C. (2017). A comprehensive biomass burning emission inventory with high spatial and temporal resolution in China. *Atmospheric Chemistry and Physics*, *17*(4), 2839-2864. https://doi.org/10.5194/acp-17-2839-2017
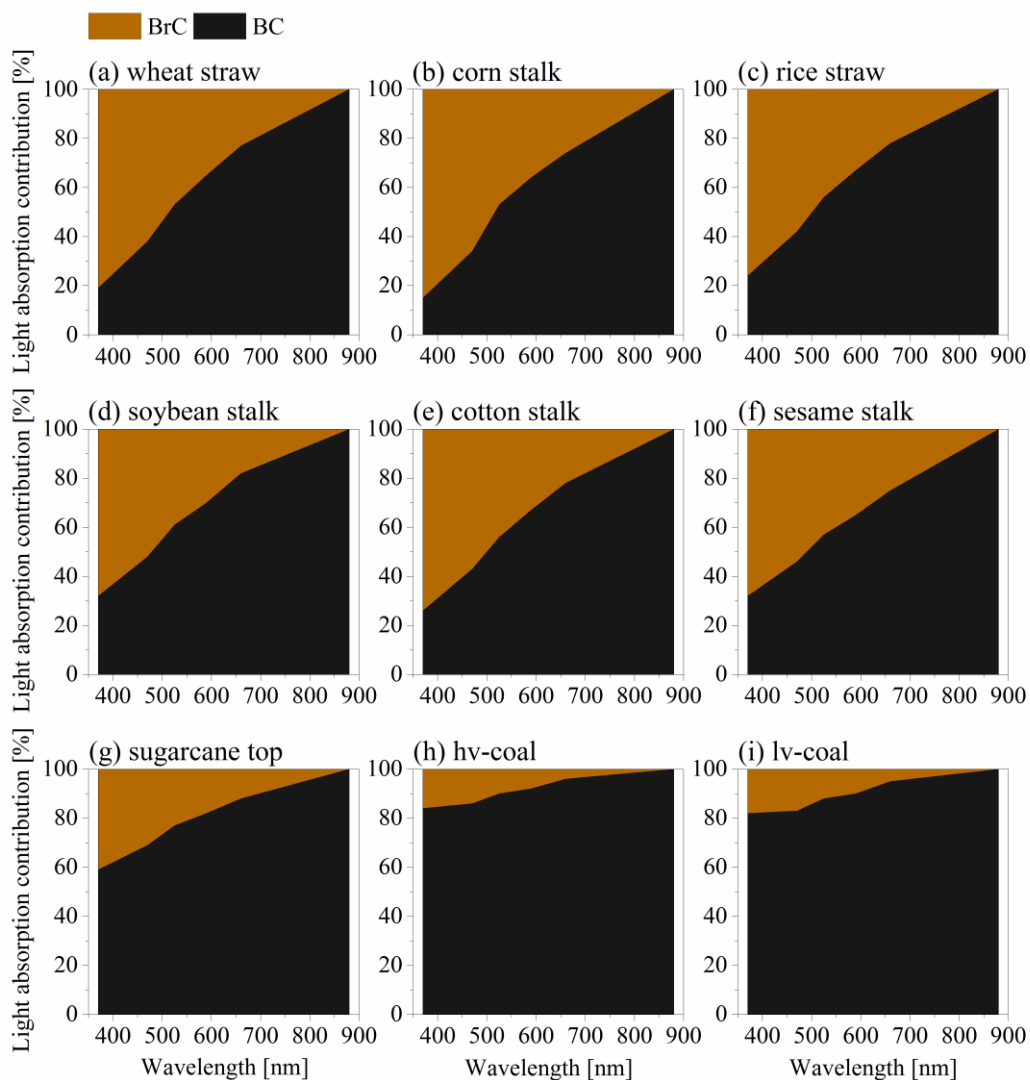
Figure 1. Fractions of light absorption at specific wavelengths by brown carbon (BrC) and black carbon (BC) in the total particles from burning of biomass and bituminous coal: (a) wheat straw, (b) corn stalk, (c) rice straw, (d) soybean straw, (e) cotton stalk, (f) sesame stalk, (g) sugarcane top, (h and i) high volatile and low volatile bituminous coals (hv-coal and lv-coal, respectively).
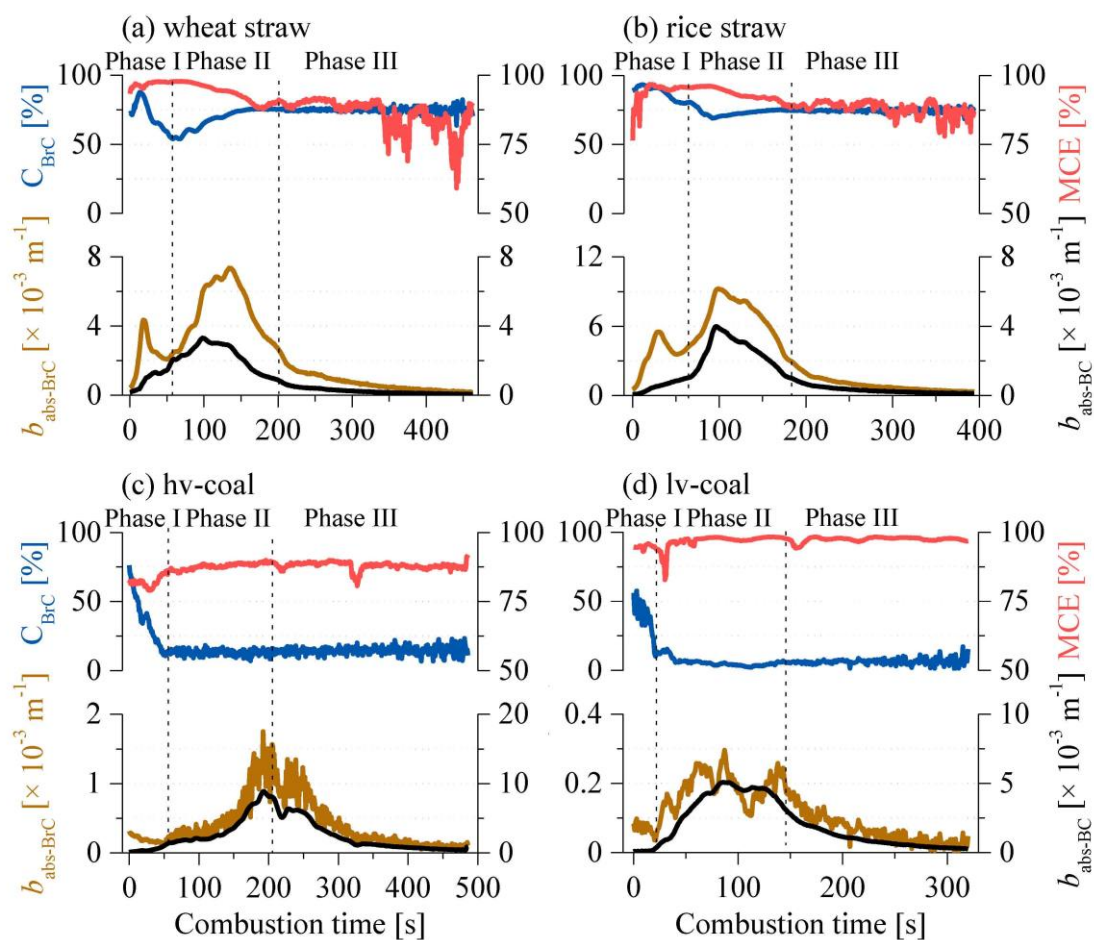
Figure 2. Time series of light absorption coefficients for brown carbon (BrC) ($b_{abs-BrC}$) and black carbon (BC) (b_{abs-BC}) at 370 nm, light absorption contribution of BrC to the total light absorption (C_{BrC}), and modified combustion efficiency (MCE) during burning of (a) wheat straw, (b) rice straw, (c and d) high volatile and low volatile bituminous coals (hv-coal and lv-coal, respectively). Time resolution is 1 s.
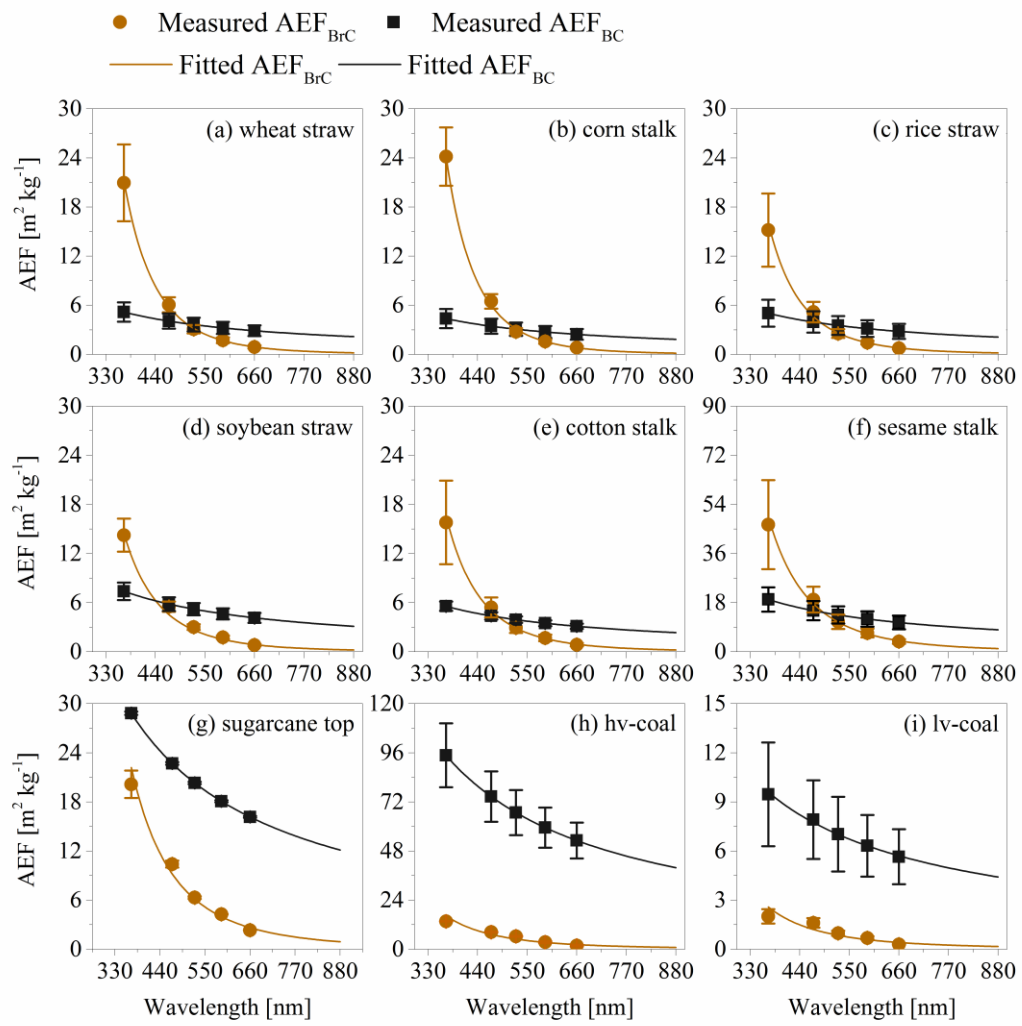
Figure 3. Absorption emission factor (AEF, in m^2 kg^{-1}) from selected crop residues and bituminous coal burning emissions.
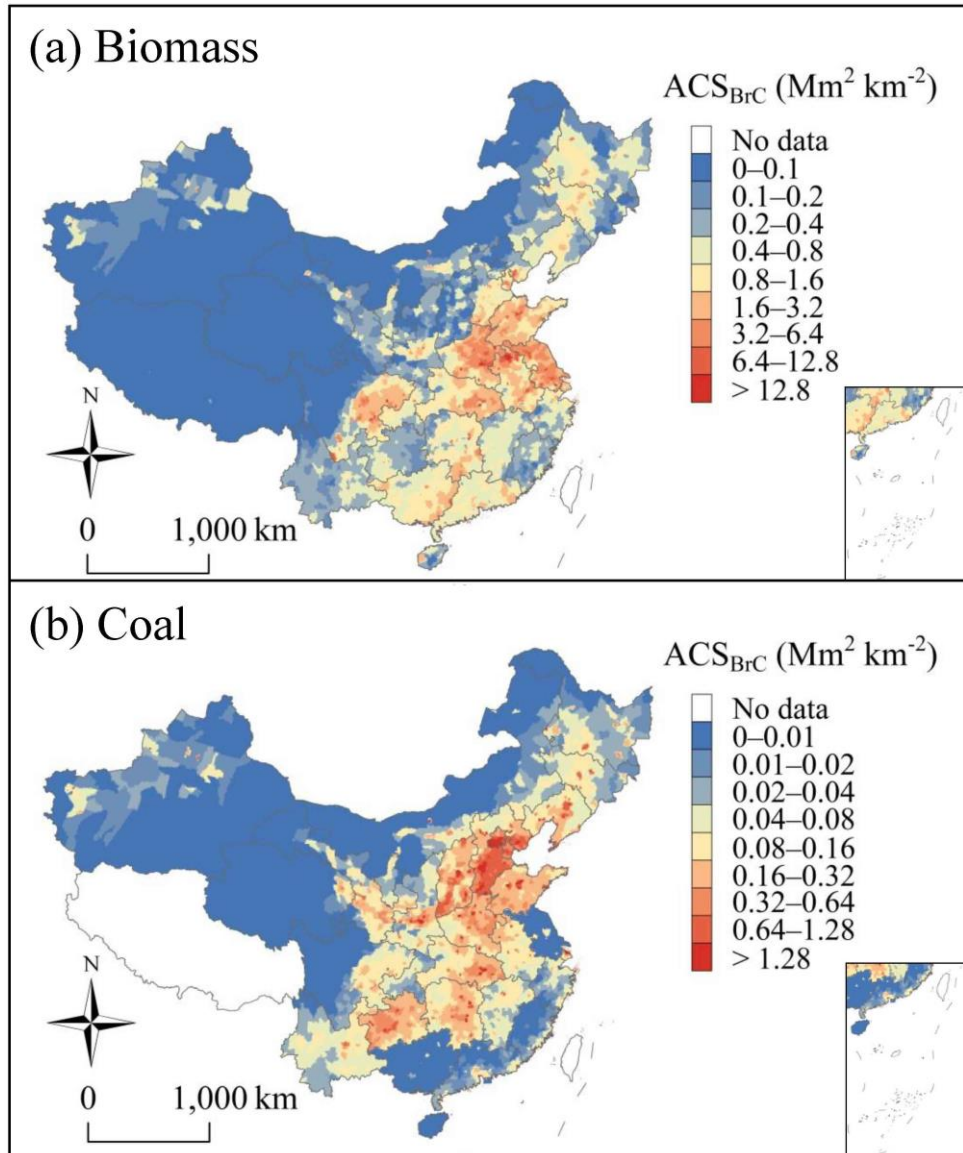
Figure 4. The geographic distributions (10 km × 10 km) of BrC absorption cross section (ACS$_{BrC}$) emissions from (a) biomass and (b) residential coal burning for China in 2015.
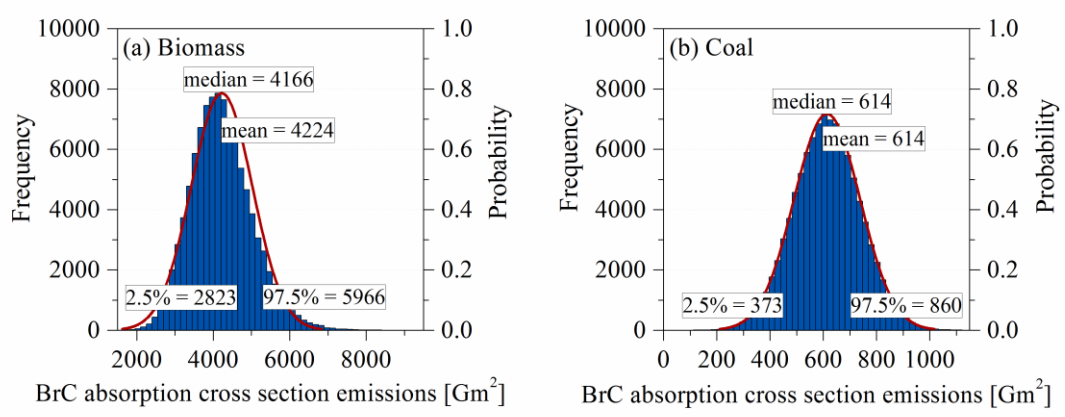
Figure 5. Probability distribution of China's national BrC absorption cross section (ACS_{BrC}) emissions in 2015, based on 100,000 Monte Carlo simulations. (a) Biomass and (b) Coal.